

Spectral Rotation in Pulsed ESR Spectroscopy*

JOSEPH P. HORNAK

Department of Chemistry, Rochester Institute of Technology, Rochester, New York 14623

AND

JACK H. FREED

Baker Laboratory of Chemistry, Cornell University, Ithaca, New York 14853

Received October 29, 1985

The technique of pulsed Fourier transform NMR spectroscopy is well developed and understood. The equivalent technique for ESR has been slower to be developed, but recent developments in ESR instrumentation have now made FT ESR possible. In this paper we consider the requirements for rotating the magnetization associated with an ESR spectrum by a microwave pulse. In addition, techniques for reconstructing the frequency (field)-domain spectrum from the time-domain spectra are described. These techniques are applied to obtain a FT spectrum from the electron spin-echo decay of γ -irradiated quartz and a FT spectrum from the free induction decay of the 2,5-di-*t*-butyl-*p*-benzosemiquinone radical recorded in 50 and 25 ms, respectively, of real time. © 1986 Academic Press, Inc.

I. INTRODUCTION

Modern Fourier transform and two-dimensional magnetic resonance techniques are based upon irradiating the spectrum with a resonant radiofrequency or microwave field. Ideally, one wishes to rotate the magnetization due to all portions of the spectrum by an equal angle, θ . In actual experiments it is not always possible to achieve this ideal, and different portions of a spectrum are rotated by different amounts depending on the extent to which they deviate from the resonance condition associated with the applied electromagnetic radiation (EMR). These matters are generally well understood in NMR (1), for which the modern FT and 2D techniques have been well-developed, but they appear to be inadequately understood in ESR. However, such matters are becoming increasingly relevant to ESR with the development of low Q , high B_1 resonators (2-4) in electron spin-echo (ESE) spectroscopy. In fact, it is becoming increasingly practical to rotate the magnetization from an entire ESR spectrum with a microwave pulse (3).

In this paper we wish to review the considerations regarding FT spectroscopy with a particular view to those that are relevant for pulsed ESR, given its current technical

* Supported by NSF Grant CHE8319826 and NIH Grant GM-25862.

possibilities and limitations. We also demonstrate them with some experimental examples.

Let us now describe the appropriate approach by first considering simplified points of view. We use the standard convention that at equilibrium the magnetization $\mathbf{M} = M_z \hat{\mathbf{k}}$, i.e., is parallel to the applied static magnetic field $\mathbf{B} = B \hat{\mathbf{k}}$. The applied EMR with angular frequency $\omega_0 = 2\pi\nu_0$, which is applied along the x axis, is resolved into two counter-rotating components, only one of which is (near)-resonant. This component is static along the x' axis rotating in the xy plane at frequency ω_0 . A pulse of EMR, applied for a period t will rotate the magnetization exactly at resonance by the angle (in radians):

$$\theta = \gamma B_1 t \quad [1]$$

about the x' axis. Here γ is the gyromagnetic ratio of the spin- $\frac{1}{2}$ particle. With a spectrum of finite extent it is no longer true that "a $\pi/2$ pulse" (according to Eq. [1]) will rotate all portions of the spectrum by $\pi/2$. A very simple "rule of thumb" is that a $\pi/2$ pulse of microwave field strength B_1 will rotate " B_1 gauss" worth of spectrum by $\sim 90^\circ$. More exactly the rotation angle is a function of ω and is about the effective $\mathbf{B}_1(\omega)$ vector with magnitude:

$$B_{\text{eff}}(\omega) = [B_1(\omega_0)^2 + ((\omega_0 - \omega)/2)^2]^{1/2}. \quad [2]$$

The rotation angle about $B_{\text{eff}}(\omega)$ is $\theta(\omega) = \gamma B_{\text{eff}}(\omega)t$. The resultant magnetization vector \mathbf{M} in the rotating frame coordinate system as a function of the initial magnetization $\mathbf{M}_0(\omega)$, is (13):

$$\mathbf{M}(\omega) = [\mathbf{M}_0(\omega) \cdot \hat{\mathbf{h}}] \hat{\mathbf{h}} + [\mathbf{M}_0(\omega) - [\mathbf{M}_0(\omega) \cdot \hat{\mathbf{h}}] \hat{\mathbf{h}}] \cos \theta - [\hat{\mathbf{h}} \times \mathbf{M}_0(\omega)] \sin \theta \quad [3]$$

where $\hat{\mathbf{h}}$ is the unit vector along $B_{\text{eff}}(\omega)$. Alternatively we may FT a square pulse of EMR extending from $t = 0$ to t to obtain the Fourier component of magnetic field:

$$B_1(B) = |B_1| \left[\frac{\sin(\gamma t(B_0 - B))}{(\gamma t(B_0 - B))} + i \frac{\sin^2(\gamma t(B_0 - B)/2)}{(\gamma t(B_0 - B)/2)} \right]. \quad [4]$$

Here $|B_1|$ is the magnitude of the rotating field, and the real (imaginary) part of Eq. [4] is along the rotating x' (y') axis. In obtaining Eq. [4] we have equated $\omega_0 = \gamma B_0$ and $\omega = \gamma B$. Equation [4] shows that an "effective" B_1 actually varies continuously from its maximum at resonance (i.e., $B_0 = B$). If we choose the pulse width to satisfy Eq. [1], valid for resonance, then we may replace γt in Eq. [4] by θ/B_1 to obtain how the "effective" B_1 varies with the magnitude of B_1 . In this form of Eq. [4] it is clear that by increasing B_1 (and correspondingly decreasing t), $B_1(B)$ will vary less over the spectrum.

The correct way to deal with this matter is, of course, to explicitly solve the quantum-mechanical equations of motion for a spin in the combined B and B_1 fields (5). More generally, we must include the effects of relaxation. In many cases the Bloch equations will apply, and one may integrate them directly (6a). In the usual notation we have

$$du/dt = -u/T_2 - (\omega - \omega_0)v \quad [5]$$

$$dv/dt = -v/T_2 - \gamma B_1 M_z + (\omega - \omega_0)u \quad [6]$$

$$dM_z/dt = -(M_z - M_{z0})/T_1 + \gamma B_1 v. \quad [7]$$

Here u , v , and M_z are, respectively, the x' , y' , and z components of magnetization. T_1 is the spin-lattice relaxation time, T_2 the homogeneous spin-spin relaxation time, and ω the Larmor frequency of an electron at resonance in a magnetic field B . With the aid of these equations, the transverse magnetization present after the application of a square pulse of microwaves with frequency ω_0 and field strength B_1 can be determined. The u and v components of magnetization thus calculated represent the respective in- and out-of-phase amounts of magnetization rotated by the pulse and expressed as a function of ω . The results for the limit where T_1 and T_2 are long relative to t approximately match those described by Eq. [4]. With the appropriate form of B_1 as a function of time, Eqs. [5]–[7] describe the effects of a multi pulse sequence on the magnetization. Note that if there is significant inhomogeneous broadening present, then the Bloch equations [5]–[7] will have to be convoluted with the shape function for the inhomogeneous broadening. For the particular case of a Lorentzian shape function, of width $T_2^{\dagger-1}$, this will lead to an effective $T_2^{*^{-1}} = T_2^{-1} + T_2^{\dagger-1}$ in the initial FID and in the spin-echo decay discussed in the next section, cf. Ref. (6b).

In reality, due to finite switching speeds (time constant $T' \simeq 10$ ns) of the microwave switches used to produce the microwave pulses and to the finite time required to form and remove power from a microwave cavity with a given Q , one should include a pulse shape function, $B_1(t)$, into the above equations to calculate the transverse magnetization. For microwaves with a magnetic field strength B_1 turned on between time $t = 0$ and t_1 , $B_1(t)$ is given by

$$\begin{aligned} B_1(t) &= 0 & \text{for } t &\leq 0 \\ B_1(t) &= B_1(1 - \exp(-t/T'))(1 - \exp(-t\omega_0/Q)) & \text{for } 0 &\leq t \leq t_1 \\ B_1(t) &= B_1(t_1)\exp(-t/T')\exp(-t\omega_0/Q) & \text{for } t &> t_1. \end{aligned} \quad [8]$$

Of equally great importance in calculating the effects of a pulse on the magnetic moments is the distribution of B_1 in the sample. A distribution in the magnitude of B_1 will cause a corresponding distribution in rotation angle as described by Eq. [1]. Ideally B_1 should be constant along the sample axis in the sample cavity, in order that all spins of a given resonant frequency are rotated by the same angle.

In the spectral reconstruction section of this paper (Section II) we describe the rotation of spectral magnetization by different pulse shapes. Also addressed, is the procedure for transforming the resultant time domain spectrum into a field-domain spectrum by the application of separate phase and amplitude corrections. We have attempted to summarize some of the major instrumental requirements in Section III. In Section IV these instrumental techniques and transformations are applied to two simple ESR spectra. A summary appears in Section V.

II. SPECTRAL RECONSTRUCTION

In time-resolved magnetic resonance spectroscopy, two general categories of pulse experiments exist, viz., the free induction decay and the spin echo. The FID sequence employs a 90° pulse of EMR immediately after which the signal is recorded. The echo sequence moves the signal or echo away from the pulses, e.g., in the $90^\circ - \tau_1 - 180^\circ - \tau_2$ -echo sequence the maximum signal is approximately at τ_2 away from the last pulse.

In general, both pulse sequences contain the same basic information about the spin system (but see below). Information about the dynamics of the spin system is, however, more readily obtained from the echo sequence than in the FID. In general an FID will be seen when the inhomogeneous T_2^* is much greater than the spectrometer dead-time t_d , which is not always the case. Due to this deadtime after the application of a pulse of EMR (7), FIDs cannot be observed for all systems. These systems are frequently those in which spin echoes can be observed. Echoes will be seen in samples when the homogeneous $T_2 \geq 2t_d$. In many samples in which there is substantial inhomogeneous broadening, it is often true that $T_2 \gg T_2^*$, so it is often possible to see echoes. In fact, since the echo width $\sim T_2^*$ (i.e., the effective T_2 , cf. Section I), it will be relatively sharp and intense when this inequality holds, so this is a favorable condition for detecting echoes. Electron spin-echo spectroscopy has evolved as the more popular form of pulsed ESR spectroscopy due to the nature of the systems investigated and instrumental constraints.

We can analyze the case for a one-pulse FID or a two-pulse ESE from the Bloch equations [5]–[7] by recognizing that the absorption signal is proportional to v , while the dispersion, detected along x' , is proportional to u . That is, in-phase detection gives u and out-of-phase, v . The transverse magnetization present immediately after the application of a 29.75 ns, 3 G 90° square pulse, as a function of $\nu = \omega/2\pi$, was calculated from Eqs. [5]–[7]. This is a case of homogeneous broadening, i.e., $T_2^* = T_2$. Figure 1 represents the case with $T_1 = T_2 = 1 \mu\text{s}$. Much of the magnetization from spins away from those which resonate at ν_0 , is located along the x' axis after the application of the 90° pulse (Fig. 1b). The similarities between Figs. 1b and c and, respectively, the real and imaginary parts of part of Eq. [2] should be noted. Quadrature detection (8) (simultaneous detection of both u and v components of magnetization) coupled with the proper form of signal reconstruction based on the shapes of the curves in Figs. 1b and c expands the width of a spectrum which might be recorded from a square pulse. A better representation of the amount of detectable signal is the resultant transverse magnetization,

$$M(\nu) = (v(\nu)^2 + u(\nu)^2)^{1/2} \quad [9]$$

shown in Fig. 1d. The amount of spectrum rotated by greater than 65° (transverse magnetization greater than 0.9) is equivalent to $B_1 (B_1\gamma/2\pi \text{ s}^{-1})$ worth of static magnetic field.

The above example represents an idealized situation, since in reality $B_1(t)$ is not a square pulse but rather a function of the form described by Eq. [8]. As an example, Fig. 2 represents the transverse magnetization present in a spectrometer with a $Q = 100$ and an infinitely fast microwave switch. Parameters such as T_1 , T_2 , and the pulse width were kept at the values in the previous example. Since there is no sharp termination to such a pulse in terms of the B_1 inside the cavity, the three lines in each figure represent the magnetization at 0, 5, and 10 ns after t_1 . The complexity of these curves would make the reconstruction of an ESR spectrum very difficult.

The use of a specially tailored pulse, which will produce a flat transverse magnetization curve over a width equivalent to a typical ESR spectrum, would simplify the reconstruction process. Such a function is the apodised sinc function ($\text{sinc}(x)/x$) (9, 10) commonly used in FT NMR spectroscopy. Figure 3 represents the transverse magnetization resulting from the application of a $\text{sinc}(x)$ function pulse where $-3\pi \leq x$

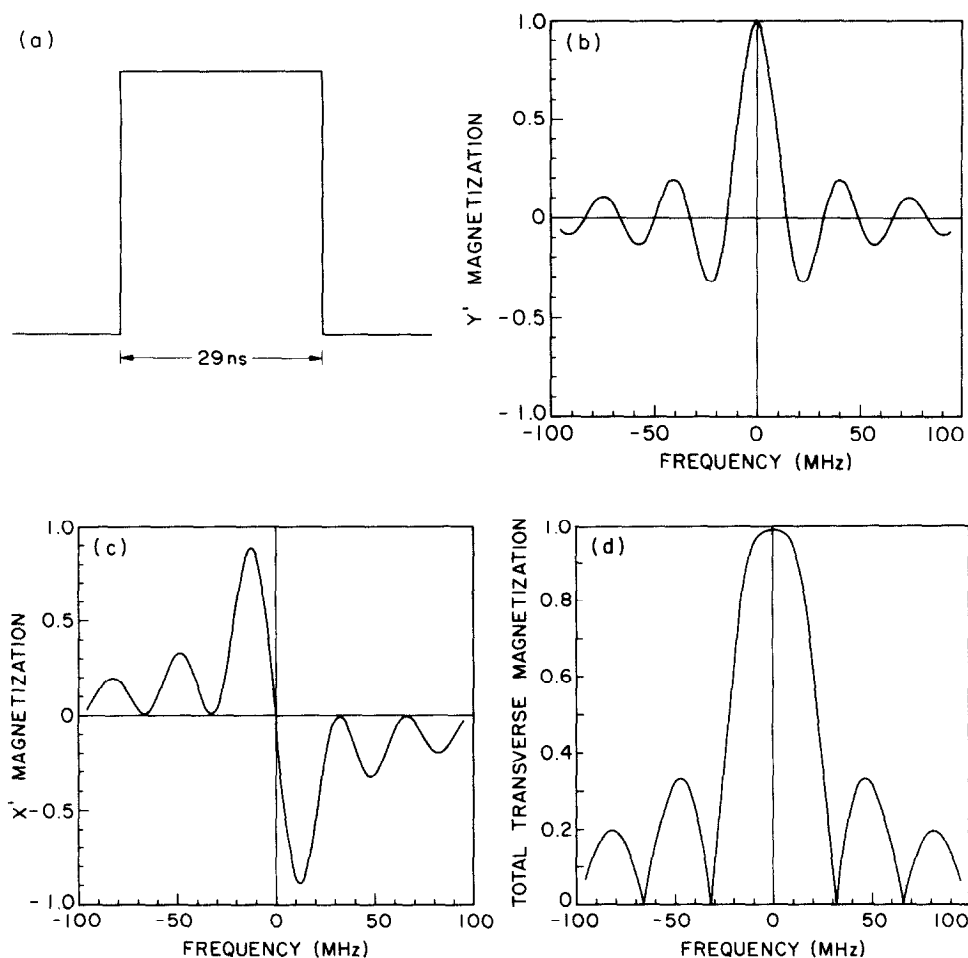


FIG. 1. Transverse magnetization resulting from the application of a square 29.75 ns $\pi/2$ pulse of B_1 at frequency ν_0 (a) to an electron spin system as a function of frequency offset from ν_0 . The curves were calculated from a numerical integration of the Bloch equations with $T_1 = T_2 = 1 \mu\text{s}$, $B_1 = 3 \text{ G}$, and initially all magnetization along the z axis. The various components of magnetization in the rotating frame are v along the y' axis (b) u along the x' axis (c) and total transverse magnetization $(u^2 + v^2)^{1/2}$ (d).

$\leq 3\pi$. The maximum effective B_1 (i.e., $B_1(\nu_0)$) was 13 G, and 6π corresponded to 45 ns. As the microwave pulse becomes more like a $\text{sinc}(x)$ pulse, the transverse magnetization becomes more like a square pulse (the FT of a sinc function). The width of the pulse is approximately $4\pi/t$, where t is the time between the $-\pi$ and π points of the sinc pulse.

As previously mentioned, quadrature detection should be employed to expand the range of signal detection and also to improve S/N . The time-domain signal is Fourier transformed to obtain the frequency-domain spectrum. Fast Fourier transform (FFT) routines require a real and an imaginary input and give a real and imaginary output array. If only v , the out-of-phase component of magnetization, is recorded, then it is typical to use it as the real entry into a FFT routine and an array of zeroes as the

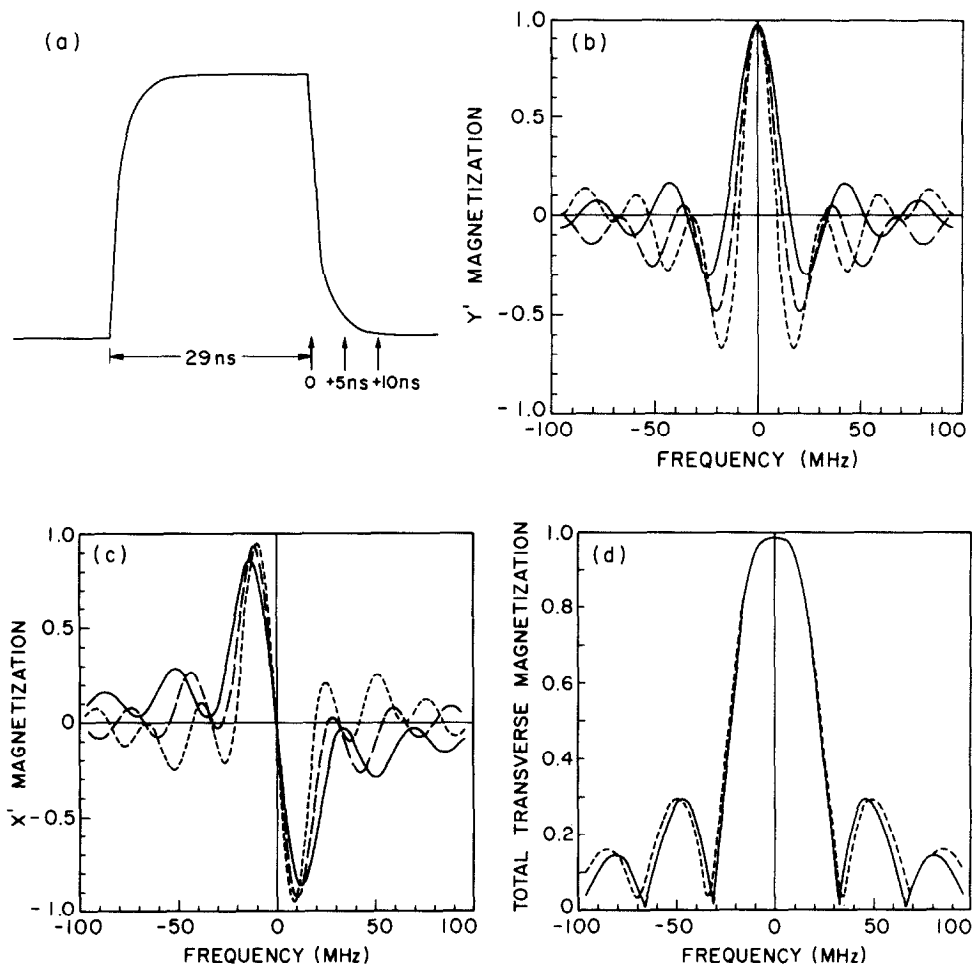


FIG. 2. Transverse magnetization resulting from the application of an exponentially rising and falling 29.75 ns $\pi/2$ pulse of B_1 at frequency ν_0 (a), typical of a square pulse sent into a cavity with a $Q = 100$, to an electron spin system as a function of frequency offset from ν_0 . The magnetization at 0, 5, and 10 ns after the turn off of the pulse is represented by the (—), (---), and (· · ·) lines, respectively. The curves were calculated from a numerical integration of the Bloch equations with $T_1 = T_2 = 1 \mu\text{s}$, $H_1 = 3 \text{ G}$, and initially all magnetization along the z axis. The v , u , and total transverse magnetization are represented in (b), (c), and (d), respectively.

imaginary entry. With these input arrays the FFT is not capable of distinguishing any difference between frequencies below and above ν_0 . The resultant spectrum is even about ν_0 and therefore appears symmetric. When u is used as the imaginary input to the FFT routine, its resultant spectrum is odd or antisymmetric about ν_0 . The output of the FFT routine in this case is the sum of these two curves and is a spectrum which distinguishes any asymmetries about ν_0 . This summation results in an improvement in the S/N ratio of the resultant spectrum assuming the noise is random. If the time dependence of v and u are used as the real and imaginary parts respectively of the input to the FFT routine, then the absorption and dispersion spectra will be the re-

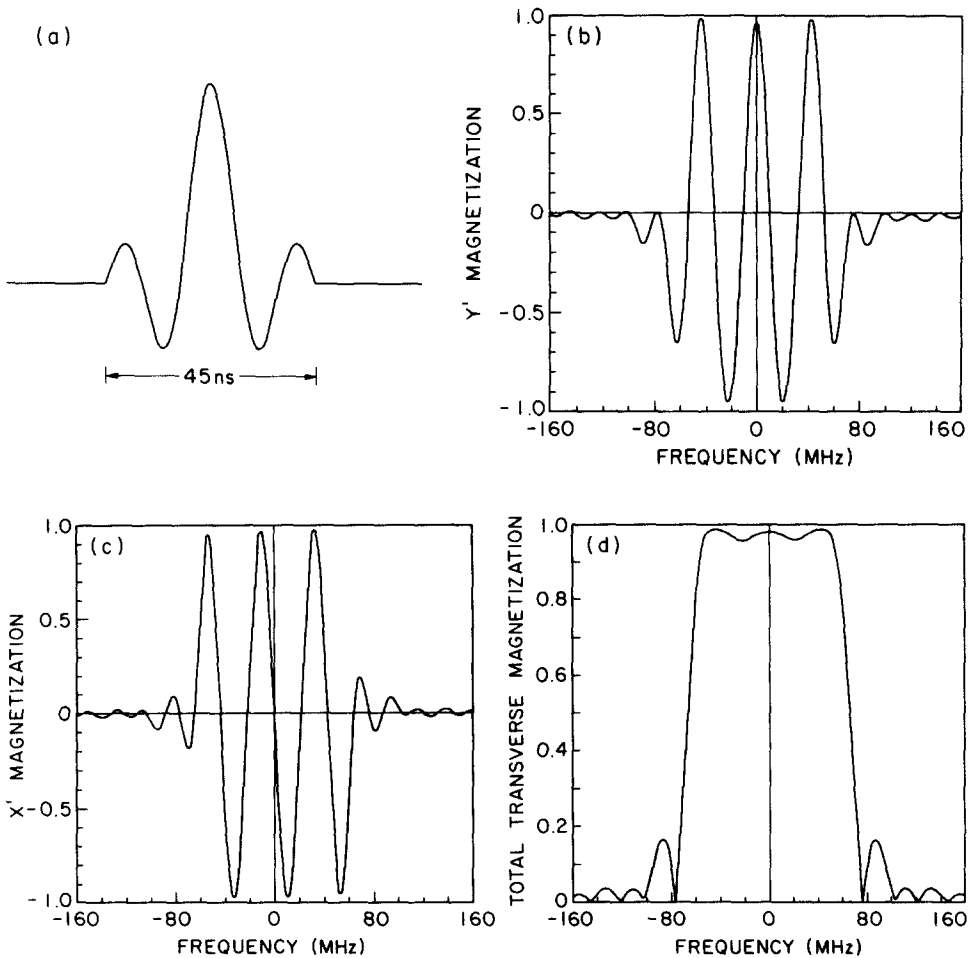


FIG. 3. Transverse magnetization resulting from the application of an apodised sinc function (see text) $\pi/2$ pulse of frequency ν_0 (a) to an electron spin system as a function of frequency offset from ν_0 . The amounts of initial z magnetization $M_z(\nu)$ rotated into the y' axis, x' axis, and $x'y'$ plane are shown in (b), (c), and (d), respectively.

spective real and imaginary outputs. Collection of components of magnetization offset from the x' and y' axes by an angle α rather than the exact x' and y' components will result in spectra which are admixtures of absorption and dispersion. This problem is easily corrected by the use of a simple coordinate transformation on the real and imaginary outputs of the FFT.

$$\begin{vmatrix} \text{Re}[S(\nu)] \\ \text{Im}[S(\nu)] \end{vmatrix} = \begin{vmatrix} \cos(\alpha) & \sin(\alpha) \\ -\sin(\alpha) & \cos(\alpha) \end{vmatrix} \begin{vmatrix} \text{Re}[S(\nu)]' \\ \text{Im}[S(\nu)]' \end{vmatrix}. \quad [10]$$

The resultant spectrum from the FFT conversion has several experimental artifacts such as that from improper phasing of the x' and y' axes just described. These artifacts can be classed as those modifying the phase of the signals and those affecting the

intensity. Both artifacts can be corrected for in the output arrays of the FFT, but the phase corrections must be applied before amplitude corrections.

The following discussion applies primarily to a 90° FID sequence. Phase adjustments can be classed as zeroeth, first, and second order and all are corrected for by the use of Eq. [8]. Zeroeth-order or constant phase corrections, where α equals a constant, usually result from improper adjustment of the detector to detect the true x' and y' magnetization. A first-order or linear phase correction, which is needed for FID but not echo techniques, is necessitated because of loss of early data points in the time-domain curve due to instrumental deadtime. Each point lost results in a linear phase deviation of π across the resultant frequency-domain spectrum (I), so $\alpha = \pi\nu/\Delta t$ where Δt is the time interval between digitized points. In an FID pulse sequence, second-order phase corrections are trigonometric in nature, and they arise from the distribution of the resultant transverse magnetization after a 90° pulse in the $x'y'$ plane as a function of frequency offset from ν_0 . The phase correction angle α is equal to the angle between the resultant transverse magnetization and the y' axis immediately after the 90° pulse. The approximate form of the frequency dependence of this angle after the application of a square $\pi/2$ pulse is given by $\tan^{-1}(\text{Im}(\text{Eq. [4]})/\text{Re}(\text{Eq. [4]}))$ and is shown in Fig. 4a. This implies that the initial u and v components have the same ratio as the Im and Re parts of Eq. [4].

The form of this function is best understood by looking at the path the transverse magnetization vector takes in the $x'y'$ plane as a function of offset from frequency ν_0 (Fig. 4b). The intensity correction adjusts the height of the lines in the resultant absorption spectrum for rotations of components of magnetization by less than 90° . It is accomplished by dividing the phase-corrected absorption spectrum by the resultant transverse magnetization function (Eq. [9]), which for a perfect square pulse is $\cong |\text{sinc}(\pi t(\nu - \nu_0))|$. These corrections are important in deuterium NMR (11), where the spectral width is large relative to the frequency-domain spectrum of the 90° pulse, and in NMR, when the carrier frequency is substantially off resonance (12, 13). The trigonometric and intensity corrections are generally not applied in conventional proton pulsed NMR due to the broad range of the spectrum which is rotated at least 90% of the expected rotation angle. The application of all of these corrections in ESR increase the extent over which a given spectrum may be recorded in a pulse experiment. The trigonometric and intensity corrections are highly pulse-shape-dependent and, for imperfect pulses, may be difficult to implement.

The dynamics of the magnetization during a spin-echo sequence or multipulse sequence are more complex than for an FID. In a spin-echo sequence, a 90° pulse (at ω_0) is applied for a time t_1 followed by a 180° pulse (at ω_0) of length t_2 at a time τ_1 after the 90° pulse. At time $\tau_2 = (\tau_1 - 3t_1/2)$ after the 180° pulse, a maximum signal or echo is observed. Assuming the relaxation times are large relative to the time of the experiment, the 90° pulse rotates magnetization by an angle $(\gamma B_{\text{eff}} t)$ about $B_{\text{eff}}(\omega)$, which is directed off the z axis in the $x'z'$ plane, by an angle $\tan^{-1}(\gamma B_1/(\omega_0 - \omega))$ as given by Eq. [1]. The location of M after a time τ_1 is $(\omega_0 - \omega)\tau_1$ radians from its position after the 90° pulse. Application of a 180° pulse at time t_1 after the 90° pulse rotates $M(\omega)$ by $\gamma B_{\text{eff}}(\omega)t_2$ about $B_{\text{eff}}(\omega)$. The pulse does not perform a reflection of all $M(\omega)$ vectors through the $x'z'$ plane as it does for $M(\omega_0)$. Therefore after a period of time τ_2 the magnetization is not identical to its value immediately after the application of the 90° pulse.

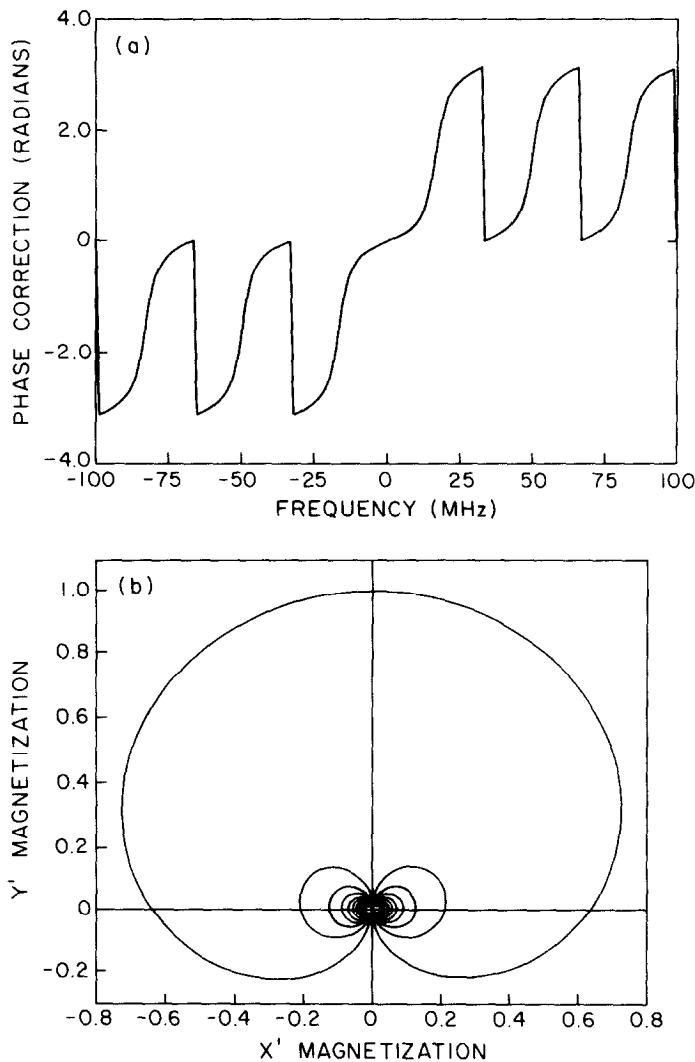


FIG. 4. (a) Frequency dependence of the trigonometric phase correction angle, the angle between the y' axis and the transverse magnetization, after the application of 30 ns $\pi/2$ pulse. (b) The lengths of the transverse magnetization vectors in the $x'y'$ plane. Distance along the length of the curve from the y' axis is equivalent to frequency offset from ν_0 . This figure explains the frequency dependence of (a).

The most appropriate way to reconstruct a frequency domain spectrum from an echo shape is to calculate the corresponding intensity and phase corrections from Eqs. [5]–[7]. For large values of τ_1 and τ_2 the resulting phase and intensity corrections for $t_1 \neq t_2$ are $(\omega - \omega_0)(t_1 - t_2/2)$ in radians and $|\text{sinc}(\pi t_1(\nu - \nu_0))\text{sinc}^2(\pi t_2(\nu - \nu_0))|$, respectively (II). For $t_1 = t_2$ the phase and intensity corrections become $(\omega - \omega_0) \times (t_1/2)$ and $|\text{sinc}^3(\pi t_1(\nu - \nu_0))|$ (Fig. 5), respectively. The interesting features of these corrections are that the phase correction is linear and that the amount of spectrum which may be conveniently reconstructed using the intensity correction factor is $\ll 2/t_1$ Hz.

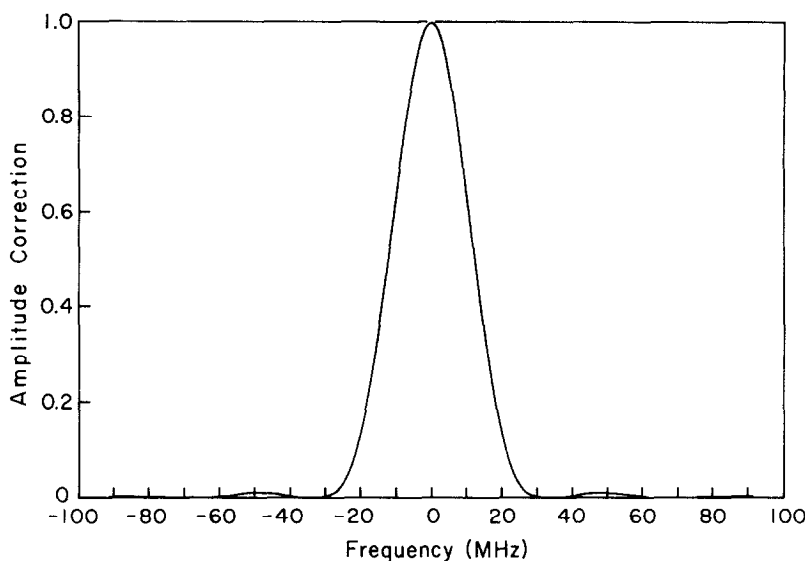


FIG. 5. The amplitude correction factor $|\text{sinc}^3(\pi(\nu - \nu_0)t)|$ for $90^\circ - \tau_1 - 180^\circ$ echo sequence where the width, t , of the 90 and 180° pulses is equal to 30 ns.

III. INSTRUMENTATION

Pulse generation for rotation of an entire ESR spectrum poses the biggest challenge in ESE spectroscopy. Perfectly square pulses of duration one to two nanoseconds or specially tailored pulses which can rotate ~ 50 G of spectrum by $\sim 90^\circ$ are desired. Minimum insertion loss and maximum isolation in the switched mode are also desired. Commercially available fast PIN diode microwave switches possess switching speeds of $\sim 2-7$ ns (14). Power-handling capability of the switches degrades with increasing switching speed. It is difficult to produce a perfectly square pulse of a few tens of nanoseconds with these switches. We have found that cascading two of these switches together could produce shorter more rounded pulses. Faster experimental microwave switches have been designed with 1 ns switching speed but lower power-handling capabilities (15). Emitter-coupled logic (ECL) switches can produce fairly square 3-4 ns pulses but have a 20 mW power-handling capability. Single-cycle (100 ps) X-band microwave pulses have been generated using experimental switches based on photoconductivity in silicon transmission-line structures (16). This switch is expected to have a 1 kW power rating with a pulsed input signal (16). Although the laser system required to pulse the semiconductor would add an extra degree of complexity to the ESE experiment, this switch represents the best prospect for short pulse generation.

Typical ESE spectrometers generate their π and $\pi/2$ pulses by varying the pulse length and keeping the pulse intensity constant. To assure rotation of equal amounts of spectrum by the two pulses and thus maximize the amount of reconstructable spectrum, the pulse width should be fixed and the pulse power of the π pulse adjusted to be four times that of the $\pi/2$ pulse. (We describe one method below). With the ratio of powers fixed, the absolute power was chosen as follows. By increasing the power from zero, the first maximum height echo was used to fix the power of the $\pi/2$ and π pulses. Higher powers would produce echoes corresponding to rotations of $(2n + 1) \times \pi/2$ and $(2n + 1)\pi$ with $n = 1, 2, 3 \dots$. The pulse power in a 90° FID sequence

was chosen such that a maximum FID intensity was produced with a minimum amount of power. This insured that the pulse was not a $(2n + 1)\pi/2$ pulse where $n = 1, 2, 3 \dots$. As an added check of the $\pi/2$ power, an $n(\pi)$ pulse gave a minimum FID. At present, specially tailored pulse shapes such as sinc functions are not conveniently produced.

Much consideration should be given to the choice of a resonator in a pulsed ESR experiment. The resonator bandwidth (ν_0/Q) should be kept high so as to pass all the frequency components of the pulse. A pulse risetime of 200 ps in the resonator requires a $Q = 5$. Distortion of the pulse shape is most evident as resonator ringing after the application of a high-power pulse. Resonator ringing increases the instrument deadtime t_d , which determines the earliest time at which data can be collected after the pulse. Overcoupling the cavity or resonator decreases the ringdown time at the expense of S/N . The loop-gap resonator (LGR) has an advantage in this respect since its high efficiency (in converting incident microwave power to B_1 in the resonator) allows the use of a lower Q , thus diminishing the ringdown time and pulse distortion. Short pulse widths are often required in two-pulse relaxation studies especially when a minimum pulse separation is desirable. When this is not the case, the optimum Q condition (rotation of the entire spectrum with minimal distortion and maximum S/N) is when the spectral width in hertz is $\leq \nu_0/2Q$, i.e., half the resonator bandwidth.¹

Ideally, the B_1 should be constant throughout the sample. B_1 along the sample axis (x axis) of a TE_{102} microwave cavity is approximately Gaussian with the maximum in the center of the cavity. Figure 6a depicts the normalized B_1 calculated by the method of perturbing spheres (17a). In ESE studies, samples are usually placed along the entire length of x axis. The $\pi/2$ and π pulse widths are adjusted to give maximum echo height, thus giving a spread in rotations from the different points along the sample. This is a major drawback to using this form of cavity in ESE experiments where complete spectral rotation is the goal. Admittedly one could use samples occupying a smaller length of the x axis, but serious attenuation of the signal-to-noise ratio would result (3) due to the lower filling factor. Another drawback with this resonator is the low efficiency of producing B_1 with incident EMR power. For an average B_1 of 3 G, approximately 200 W of power is necessary. This necessitates the use of a traveling wave tube amplifier (TWTA) to amplify the ~ 1 W from the microwave source. The slotted tube resonator (4b) has a high filling factor but a $\sin(x\pi/L)$ distribution of B_1 intensity along the sample of length L . A more suitable microwave sample cavity would be the loop-gap resonator (LGR) (2, 3). The B_1 distribution along the sample axis in this resonator is nearly uniform (Fig. 6b), thus assuring that all spins are rotated by nearly the same amount. Its superior signal-to-noise characteristics over a TE_{102} cavity for volume limited samples is another advantage in its favor (3). The high efficiency and low Q of the LGR make it ideal for use in ESE experiments where high power and short pulses are needed for complete spectral rotation.

Two important considerations concerning the data acquisition are the digitization period (i.e., time resolution) and the time over which the data are collected. The period of digitization in the time domain must be at least the reciprocal of the spread in the

¹ Although we discussed the effects of finite Q on the effective B_1 in the previous section, we did not consider its effect on attenuating the induced transverse magnetization components at ν for $|\nu - \nu_0| \geq 2Q$. This is probably best determined in an empirical fashion by studying the variation in observed signal from a narrow-line signal as $\nu - \nu_0$ is varied.

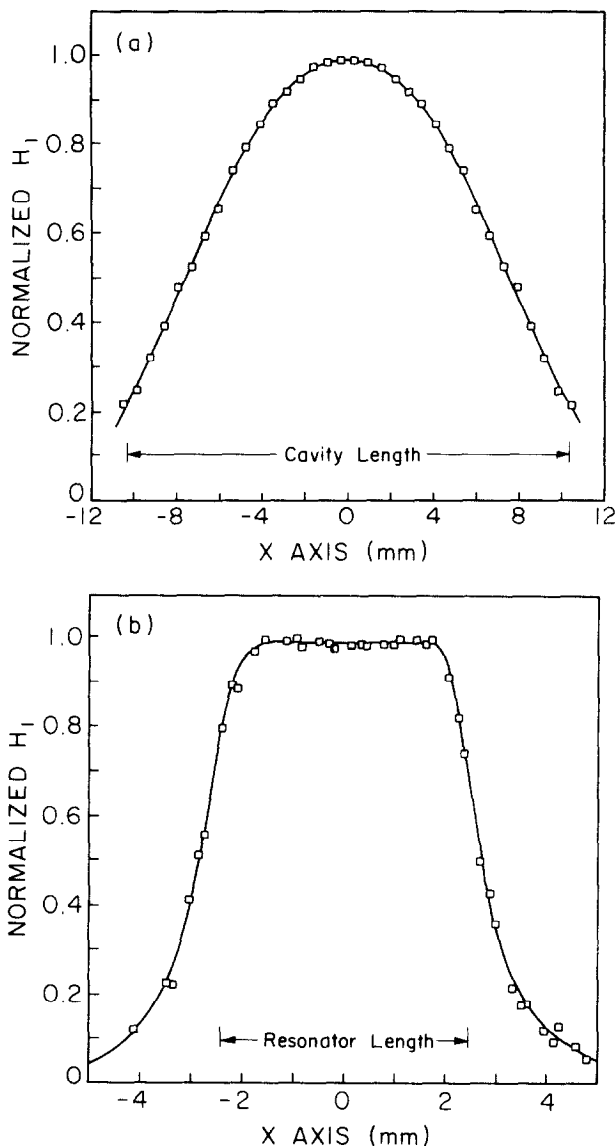


FIG. 6. Microwave magnetic field, B_1 , as a function of position along the x axis of (a) a TE_{102} microwave cavity and (b) a loop-gap resonator. Data points are B_1 calculated by the method of perturbing spheres (see text). Solid lines are drawn to guide the eye.

frequencies to be recorded in the spectrum. The resolution in the frequency-domain spectrum will be just the reciprocal of the time over which the FID is recorded. Boxcar averagers and 1 ns digital delay generators commonly found on ESE spectrometers could be used to digitize a spectrum but would be time inefficient. Transient digitizers of 5–10 ns time resolution are usable with spectra <200 – 100 MHz. Such a digitizer (e.g., the Analogic Data 6000, with which we have experimented (17b)) would allow realization of the time efficiency of the FT experiment. Digitizing the prescribed amount of data is not necessary if the echo shape or the FID has diminished to zero well before

all these data have been recorded. The typical practice in such cases is to record data until the signal has diminished to a point below the level recoverable by signal averaging and then to zero fill the remainder of the time-domain spectrum. The transition between actual data and zero-filled data should be made as smooth as possible to avoid artifacts in the frequency-domain spectrum close to ν_0 . A dc offset or a sloping baseline, due to the detector recovering from a high-power pulse, should be eliminated before performing the FT. Alternatively, linear prediction methods (17c) may be applied, especially when the FID is well represented by a sum of decaying sinusoids.

The quadrature detection scheme for maximum data throughput would be a microwave bridge with a phase shifter which could shift by exactly 90 or 180° the phase of the reference signal into the phase-sensitive detector for alternate pulse sequences. The 90° shift is for quadrature detection, and the 180° shift is for noise reduction (6, 7). The use of phase shifters with a preset 90 or 180° shift is not preferable since the phase shift varies with microwave frequency. Two examples of alternative approaches are a continuously variable phase shifter consisting of a circulator-microwave switch-tunable short combination (cf. Fig. 7), or a pair of double balanced mixers, as noted below.

IV. EXPERIMENTAL

In this section, two examples of performing FT on time-domain data are given. In one, the latter half of a spin echo is collected, and in the other a FID is collected. In conventional ESE spectrometers, the π pulse is adjusted to be twice as long in time as the $\pi/2$ pulse. To assure rotation of equal amounts of spectrum by both pulses, our basic ESE spectrometer described by Stillman and Schwartz (18) was modified to produce pulses which would differ by a factor of 2 in intensity of B_1 or a factor of 4 in power. This was accomplished by inserting a three-port circulator between the usual pulse producing switch and the TWTA (Fig. 7). The circulator directed the usual power from the pulses produced by SW1 in Fig. 7 toward another microwave switch SW2. When SW2 was open, power was reflected from this switch and circulated towards the TWTA. In the closed position of SW2, a pulse is sent through a variable attenuator towards an adjustable short, which also serves as a phase shifter, and it is reflected back through the arm and toward the TWTA. In a 90–180° pulse sequence the pulse width was generated with SW1. The 180° pulse was produced with SW2 open, while the 90° pulse with SW2 closed, thus allowing it to be attenuated by the additional arm. By measuring the pulse power emanating from the TWTA from each pulse, the proper intensity could be set. The phase shift in the attenuated pulse, due to the increased length which it must travel, was corrected by using the adjustable short with a phase sensitive detection scheme to monitor the pulses.

The repetition rate of the pulse sequences used was 1 kHz, (but 10 kHz rates could readily be used). Time-domain data were collected using a boxcar averager stepped out at 1 or 2 ns intervals. Typically 25 averages were made by the boxcar for each point recorded in the time-domain spectrum. Once the 90° out-of-phase spectrum was recorded, the phase of the microwaves in the reference arm of the spectrometer was manually changed by 90° and the in-phase spectrum recorded. The use of a more automatic phase shifter is preferred in these types of experiments, but the present setup was suitable for the present purposes with stable chemical systems. (Another alternative is to split the signal, and send it into two double-balanced mixers whose

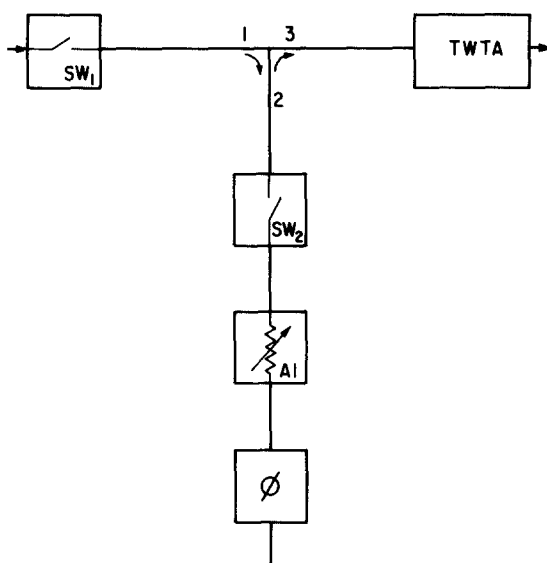


FIG. 7. A block diagram of the modifications made to the ESE spectrometer to allow it to produce variable power pulses. The modification consists of a three part circulator, a microwave switch (SW2), a variable attenuator (A1), and an adjustable short serving as a phase shifter (ϕ). The circulator was inserted between the normal low-power pulse-producing microwave switch and the input to the TWTA.

reference signal phases differ by 90° . We have previously used this approach in a 1 GHz pulse spectrometer (17b.) With a quadrature detection scheme capable of recording both the in- and out-of-phase signals simultaneously and with a transient digitizer, spectra of the intensity shown here could be recorded in ~ 25 ms of real time.

The basic loop-gap resonator described in (3) with a bandwidth of ~ 24 MHz was used in obtaining all the results. Typically, cavity resonators in ESE spectroscopy are overcoupled to minimize the cavity ringing after the application of the high-power pulses and to provide adequate signal. With the LGR, we found for these experiments that resonator ringing was not a problem and critical coupling was used. (However, overcoupling will increase the bandwidth). Samples were placed inside a 1.2 mm glass capillary such that only a length of capillary equal to the length of resonator with constant B_1 was filled.

As a demonstration of recovering an entire frequency-domain spectrum from the echo, a sample of crushed gamma irradiated quartz (E' centers with $g_{\parallel} = 2.0018$, $g_{\perp} = 2.004$) (19) was chosen. Figure 8a shows the cw absorption signal from γ -irradiated quartz as a function of frequency offset from the TE_{102} cavity resonant frequency.² Due to the short T_2^* of this sample and the large deadtime typical of most ESE spectrometers, the FID from this sample could not be FT to obtain a frequency-domain spectrum. The pulse widths were both ~ 30 ns and the total peak power needed to produce the 180° rotation was ~ 1.2 W. The pulse separation, τ_1 , was ~ 150 ns. The magnetic field and the phase of the 90° out-of-phase spectrum were adjusted, so as to

² It should be noted that the frequency representation of this spectrum is the reverse of the magnetic field domain so the high-field end of the spectrum is at the left.

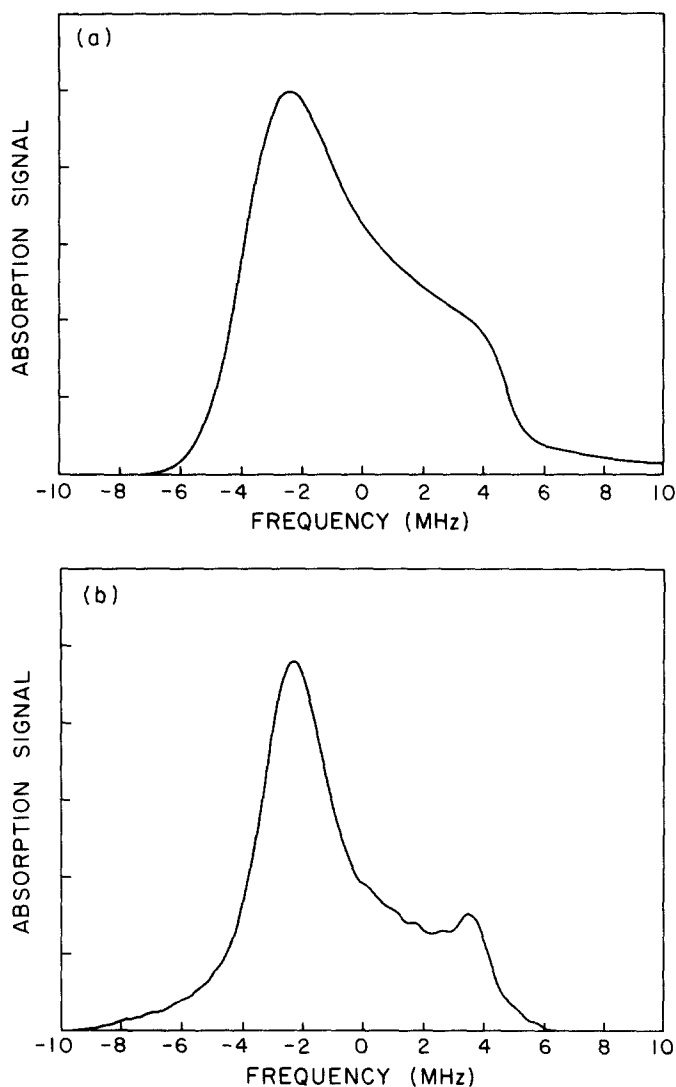


FIG. 8. The frequency-domain representation of the ESR absorption spectrum of γ -irradiated quartz ($g_{\parallel} = 2.0018$, $g_{\perp} = 2.0004$). Spectrum (a) was recorded using a TE_{102} cavity of a cw instrument with $\sim 2 \times 10^{-2}$ G, 100 kHz field modulation, and 32 mW of microwave power. Spectrum (b) was obtained using a loop-gap resonator by Fourier transforming the in- and out-of-phase latter half of the echo shape from a $90^{\circ}-\tau_1-180^{\circ}-\tau_2$ -echo sequence using pulse widths of 30 ns and $B_1 = 3$ and 6 G, respectively. The digitization period was 2 ns, and 2 μ s of data were collected and zero filled to 8 μ s. Amplitude and first-order phase corrections were applied to the transformed frequency-domain spectrum.

give the maximum symmetric echo height at a time τ_2 after the second pulse. The phase of the in-phase time-domain spectrum was adjusted so as to cause the echo height to be zero at the time when it was a maximum in the out-of-phase spectrum. The time-domain spectrum was recorded with a digitization period of 2 ns over a total time interval of 2 μ s. After a baseline correction, each curve was zero filled to 4 μ s and the FFT performed. Since data were collected starting at the middle (or maximum) of the echo, the true time zero data were included, and because the exact

in-phase u and 90° out-of-phase v spectra were recorded, only the $(\omega - \omega_0)t_1/2$ phase correction was applied. An amplitude correction of $|\text{sinc}^3(\pi(\nu - \nu_0)t_1)|$ was applied due to the relatively large frequency spectrum of the spin system (~ 10 MHz) compared with the width of the 30 ns pulse. The resultant absorption spectrum is shown in Fig. 8b. As expected, the Fourier-transformed spectrum did not look exactly like the cw spectrum may be due to differences in rate of relaxation of spectral components between the pulses and the echo.

Certain ESR spectra which are motionally narrowed and homogeneous do not show an echo.³ These in turn often exhibit an intense FID which lasts much longer than the instrument deadtime and may be FT to obtain the frequency-domain spectrum. The 2,5-di-*t*-butyl-*para*-benzosemiquinone radical anion (2,5DTBSQ) ($g = 2.0046$, $a(2\text{H}) = 2.14$ G, $a(18\text{H}) = 0.06$ G.) (20) is a radical which shows no echo but a large FID. The phasing of the 90° -out-of-phase FID was chosen so as to give the maximum intensity FID. The in-phase was adjusted so as to cause what was a maximum excursion in the out-of-phase FID at a particular time to be zero. With this radical, where the ratio of the line intensities is 1:2:1, the above condition is easy to achieve when H_0 and ν_0 are set to the resonance condition for the central line of the spectrum. In this case the in-phase FID is equal to zero and the out-of-phase signal is an all-positive or all-negative FID depending on whether the phase is $\pm 90^\circ$. The in-phase and 90° out-of-phase FIDs from the 2,5DTBSQ radical were digitized with a period of one point per ns for $1 \mu\text{s}$. The out-of- and in-phase FIDs were input into the FFT routine as the real and imaginary parts, respectively. The output real and imaginary curves were phase corrected for a net linear phase error of $(\nu - \nu_0)\pi/14$ radians where ν is in megahertz. This was composed of a contribution from unrecorded data points at the beginning of the FID and from a trigonometric correction which was nearly linear across the spectrum. Here again, the same amplitude correction factor as was used with the quartz spectrum had little influence over the width of this spectrum. The resultant spectrum is shown in Fig. 9. The shape of this spectrum is due to unresolved hyperfine lines and Heisenberg spin exchange. [To date we have obtained FT spectra from a nitroxide with a total spectral extent of 80 MHz with a 5 ns pulse width for which a $\pi/2$ pulse corresponds to $B_1 = 18$ G].

The corresponding time domain spectra of Figs. 7 and 8 were recorded in 50 and 25 ms worth of real time. We define real time as the total effective data collecting time. Each point in the time-domain spectra resulted from 25 averages. Based on similar experiments with these spin system in a TE_{102} microwave cavity, we calculate the S/N ratio to be a factor of 4 better using the loop-gap resonator. When the volume difference of the samples (3) is taken into account, this reflects a 64-fold improvement in S/N per unit volume of spins.

V. SUMMARY

In this paper we have discussed many of the aspects associated with performing pulsed FT ESR spectroscopy. Most of these are a direct carryover from FT NMR spectroscopy, where they have become so commonplace that they are now buried in automated computer software.

The application of a $\pi/2$ pulse of EMR at ν_0 to a spin system does not rotate all

³ The usual technique of introducing field inhomogeneity by the use of a ferromagnetic object in the magnetic field would produce an echo but the resultant frequency-domain spectrum would be that of the added inhomogeneity rather than the true frequency-domain spectrum.

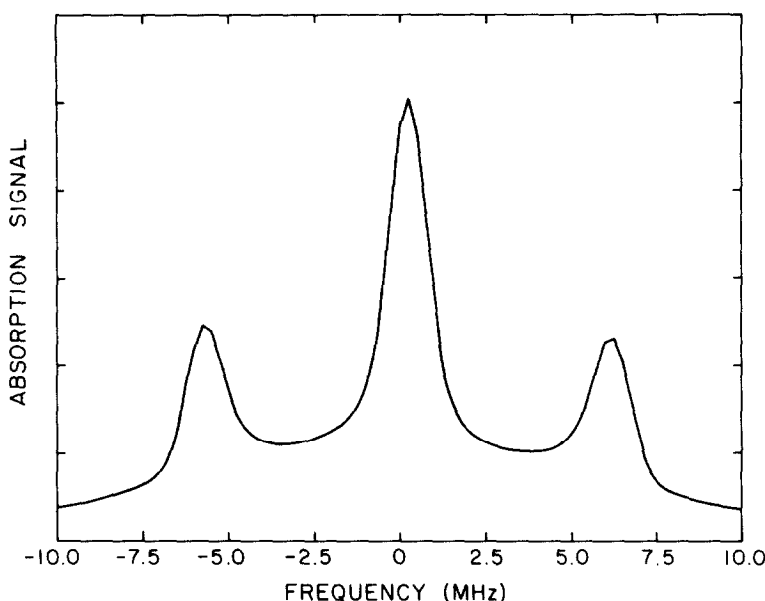


FIG. 9. The ESR absorption spectrum of the 2,5-di-*t*-butyl-*para*-benzosemiquinone radical anion [$g = 2.0046$, $a(2H) = 2.14$ G, $a(18H) = 0.06$ G]. The spectrum was obtained from the in- and out-of-phase components of the FID recorded after the application of a 30 ns pulse of $B_1 = 3$ G. The digitization period was 1 ns, and 1 μ s worth of data were recorded and then zero filled to 4 μ s. A linear phase correction of $(\nu - \nu_0)\pi/14$ radians and an amplitude correction factor of $|\text{sinc}^3((\nu - \nu_0)\pi/33.23)|$ with ν in MHz were used (see text). This spectrum is a good representation of the cw spectrum of this radical.

components of a spectrum equally. Those ν_0 are rotated by 90° about the x' axis. Other frequencies at $\pm\Delta\nu$ from ν_0 are rotated by a lesser extent, and the resultant transverse components are no longer along the y' axis, but their positions in the $x'y'$ plane may be estimated. The resultant FID or echo shape depends on these factors. Reconstruction of a frequency-domain spectrum requires both amplitude and phase corrections to the Fourier-transformed time-domain spectrum. Zeroeth- and any type of first-order phase corrections arise from instrumental features and are readily applied. In reconstructing a frequency-domain spectrum from an FID, a second-order phase correction arises from the angle between the rotated transverse magnetization (with frequencies displaced from resonance) and the y and the y' axis. In general the second-order phase corrections diverge when $t/\Delta\nu$ is an integer multiple of π . Reconstruction of a spectrum from an echo shape involves only a first-order phase correction. Amplitude corrections applied after phase corrections, account for magnetization at frequencies different than ν_0 being rotated by less than the ideal amount. The width of an ESR spectrum which may be reconstructed from an echo sequence, is less than that from an FID sequence for pulses of identical length.

The Fourier transform of echo and FID spectra need not be identical to the cw spectrum, even with the proper amplitude and phase corrections. In an echo experiment, spectral components with shorter T_2 may decay away during the period t of the pulse sequence, and thus not be present in the echo. The cw spectrum will not be affected by differences in relaxation times. A similar statement holds for the FID when some spectral components relax faster than others, and are lost during the spectrometer deadtime.

The advantages of FT ESR spectroscopy are, of course, the substantial time savings over cw techniques.

Such problems as are associated with deadspots in a spectrum reconstructed from an FID that are due to net rotations by 0° from the z axis may be overcome by performing two experiments with different pulse lengths. This would permit collection of a complete spectrum from all frequency components in that spectrum by moving the deadspot. The width limitation on the reconstructed echo spectrum may only be improved by decreasing the pulse widths (and/or by improving their shapes).

FT ESE spectroscopy would be expected to greatly increase the speed of two-dimensional ESE studies (21), since field scanning would not be necessary. It is conceivable that a 2-D spectrum recorded in 5 h by the old technique could take a few tens of minutes by the implementation of methods described here.

We have shown, in two separate examples, which are only intended to illustrate the phase and amplitude correction procedure, how an echo shape and a FID can be transformed to obtain frequency-domain spectra. These transformations, of course, require a knowledge of the true pulse shape at the sample.

REFERENCES

1. E. FUKUSHIMA AND S. B. W. ROEDER, "Experimental Pulse NMR, A Nuts and Bolts Approach," Addison-Wesley, Reading, Mass., 1981.
2. W. FRONCISZ AND J. S. HYDE, *J. Magn. Reson.* **47**, 515 (1982).
3. J. P. HORNAK AND J. H. FREED, *J. Magn. Reson.* **62**, 311 (1985).
4. Papers presented at the 8th International EPR Symposium, Denver, Colorado, 1985: (a) W. FRONCISZ AND J. S. HYDE, "Topologies of the Loop-Gap Resonator"; (b) A. GRUPP, H. SEIDEL, P. HOFER, G. G. MARESCH, AND M. MEHRING, "Design and Performance of Slotted Tube Resonators for Pulsed ESR and ENDOR"; (c) R. BOBRUTTO AND J. S. LEIGH, "Construction of a Compact X-Band Microwave Resonator for use with Liquid Helium Flow Systems"; (d) C. T. LIN, R. J. MASSOTH, J. R. NORRIS, AND M. K. BOWMAN, "Microwave Resonator Performance In Photosynthetic Pulsed EPR Experiments."
5. A. ABRAGAM, "The Principles of Nuclear Magnetism," Oxford Univ. Press, London, 1961.
6. (a) R. W. FESSENDEN, J. P. HORNAK, AND B. VENKATARAMAN, *J. Chem. Phys.* **74**, 3694 (1981); (b) L. J. SCHWARTZ, E. MEIROVITCH, J. A. RIPLEESTER, AND J. H. FREED, *J. Phys. Chem.* **87**, 4453 (1983) (Appendix B).
7. L. Kevan and R. N. Schwartz, Eds., "Time Domain Electron Spin Resonance," Wiley, New York, 1979.
8. O. E. STEJSKAL AND J. SCHAEFER, *J. Magn. Reson.* **13**, 249 (1974); **14**, 160 (1974).
9. M. S. SILVER, R. I. JOSEPH, AND D. I. HOULT, *J. Magn. Reson.* **59**, 347 (1984).
10. A. J. TEMPS, JR., AND C. F. BREWER, *J. Magn. Reson.* **56**, 355 (1984).
11. M. BLOOM, J. H. DAVIS, AND M. I. VALIC, *Can. J. Phys.* **58**, 1510 (1980).
12. R. R. ERNST AND W. A. ANDERSON, *Rev. Sci. Instrum.* **37**, 93 (1966).
13. P. MEAKIN AND J. P. JENSON, *J. Magn. Reson.* **10**, 290 (1973).
14. "Fast Switching PIN Diodes," Hewlett Packard application note 929.
15. M. C. YOUNG, H. W. PRINSEN, R. J. BLUM, AND B. R. TRIPP, *Proc. IEEE Lett.* **55**, 2185 (1967).
16. A. M. JOHNSON AND D. H. AUSTON, *IEEE J. Quantum. Electron.* **QE-11**, 283 (1975).
17. (a) J. H. FREED, D. S. LENIART, AND J. S. HYDE, *J. Chem. Phys.* **47**, 2762 (1967); (b) B. JOHNSON, Ph.D. Thesis, Cornell University, 1984; C. H. BARKHUIJSEN, R. DE BEER, W. M. M. J. BOVEE, AND D. VAN ORMONDT, *J. Magn. Reson.* **61**, 465 (1985).
18. A. E. STILLMAN AND R. N. SCHWARTZ, *J. Phys. Chem.* **85**, 3031 (1981).
19. R. H. SILSBEE, *J. Appl. Phys.* **32**, 1459 (1961).
20. B. VENKATARAMAN, Ph.D. Thesis, Columbia University, 1955.
21. (a) G. L. MILLHAUSER AND J. H. FREED, *J. Chem. Phys.* **81**, 37 (1984); (b) L. KAR, G. L. MILLHAUSER, AND J. H. FREED, *J. Phys. Chem.* **88**, 3951 (1984).